Supplement of Biogeosciences, 22, 2049–2067, 2025
https://doi.org/10.5194/bg-22-2049-2025-supplement

Biogeosciences Open Access EGU

Supplement of

Detection of fast-changing intra-seasonal vegetation dynamics of drylands using solar-induced chlorophyll fluorescence (SIF)

Jiaming Wen et al.

Correspondence to: Jiaming Wen (jwen@carnegiescience.edu) and Ying Sun (ys776@cornell.edu)

This supplementary material includes Figures S1-S12, supplementary figures to the main manuscript.

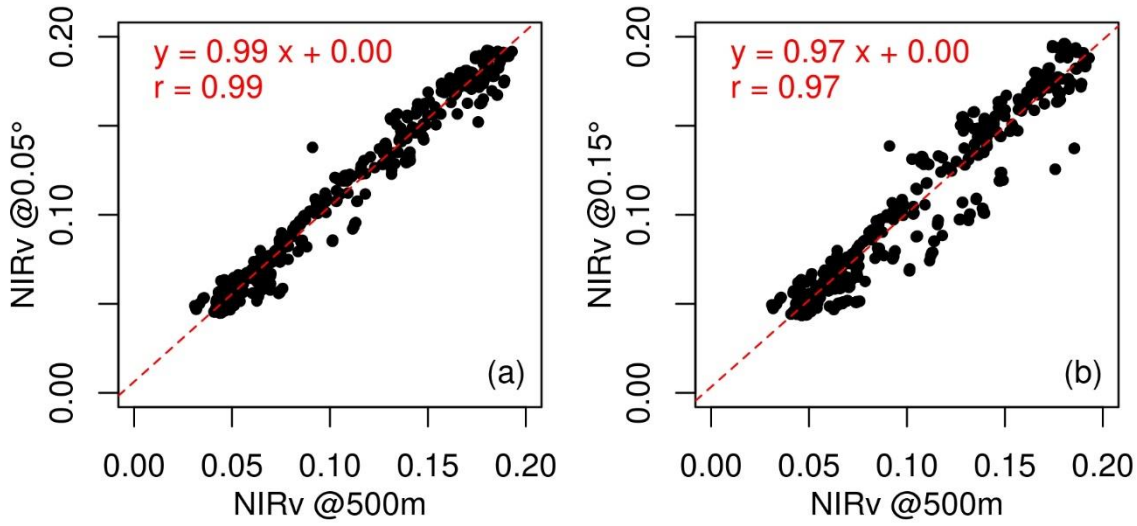

Figure S1: Comparison of daily MODIS NIRv at Kapiti extracted at (a) 500 m vs 0.05°, and (b) 500 m vs 0.15° pixels during 2019-2020. The temporal variations of different spatial scales are highly consistent.

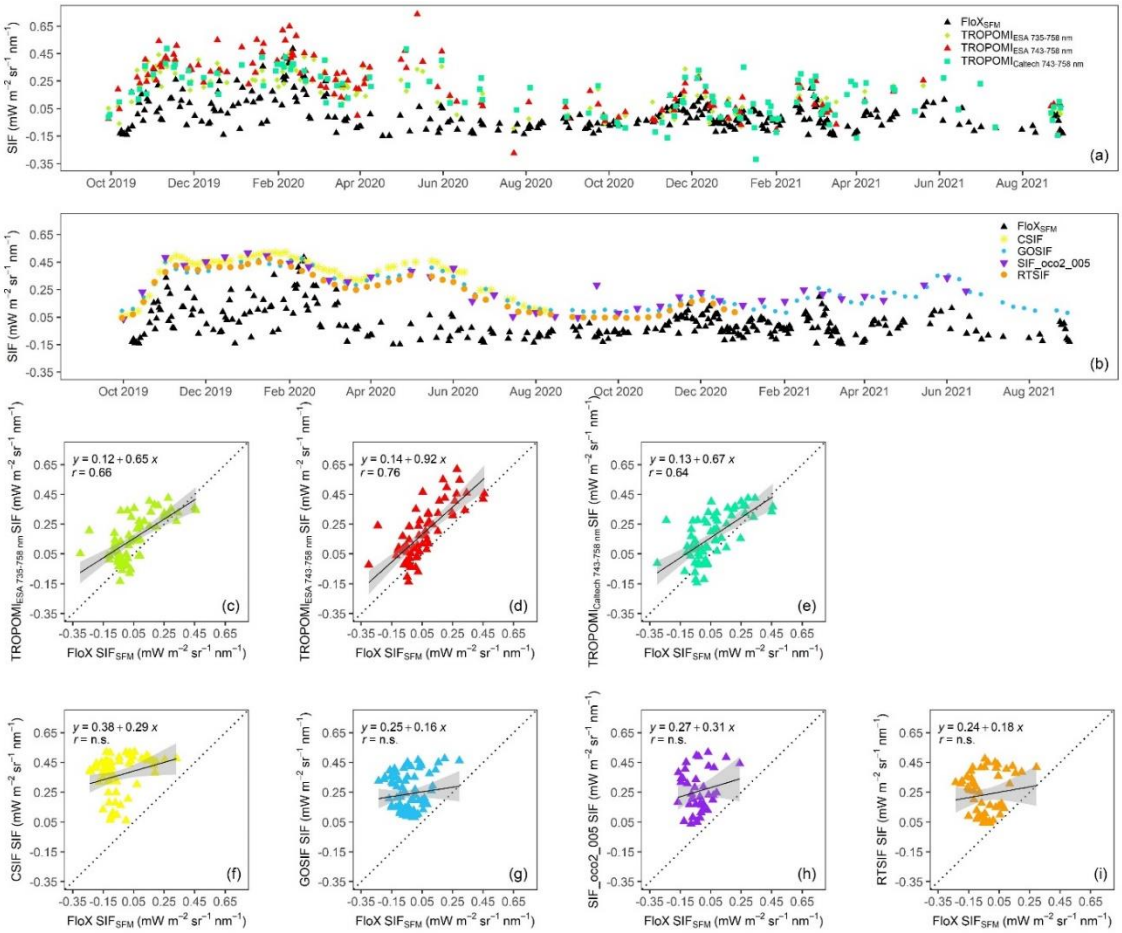

Figure S2: Similar to Fig. 2, but with FloX SIF$_{SFM}$. Not significant correlations are indicated as n.s. (p>0.05).

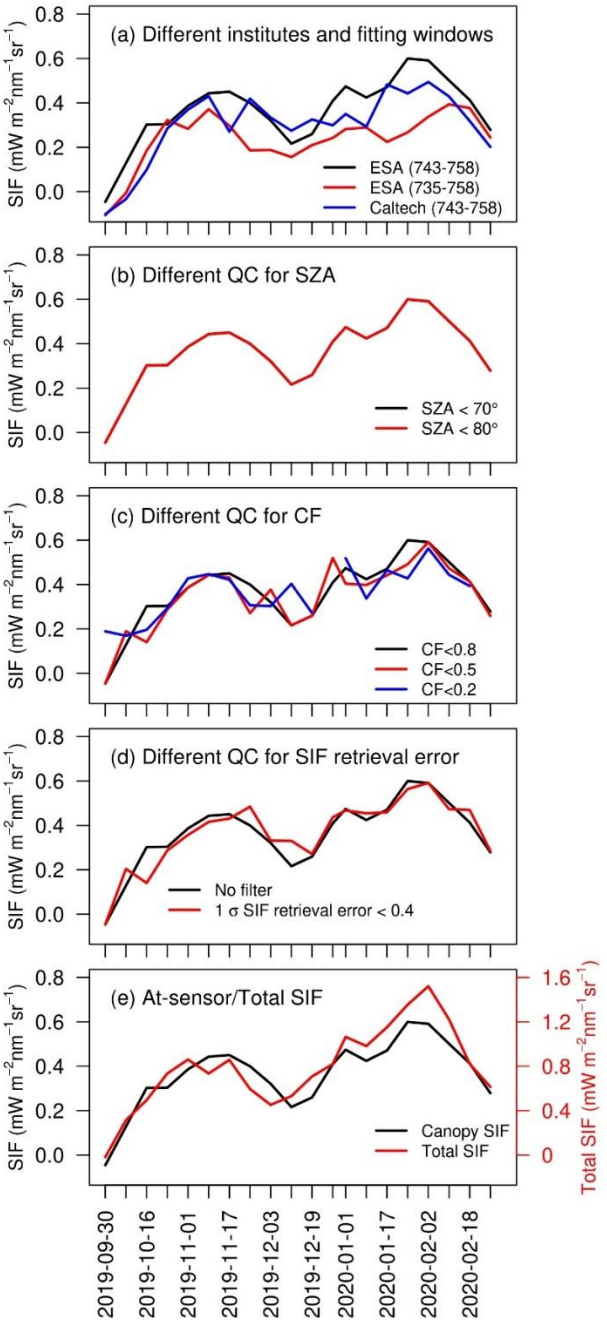

Figure S3: Sensitivity tests of TROPOMI SIF from October 2019 to February 2020, with (a) different fitting windows for SIF retrievals or data sources (ESA, Guanter et al. 2021; Caltech, Köhler et al., 2018); (b) different quality control (QC) filters for solar zenith angle (SZA) thresholds; (c) different QC filters for cloud fraction (CF) thresholds; (d) different QC filters for SIF retrieval error; and (e) whether SIF escape probability was accounted for, following Zhang et al. (2020b). Only one criterion varies for each panel relative to the baseline (used in the main analyses): ESA (743-758nm), SZA<70°, CF<0.8, at-sensor SIF. The black and red curves in (b) are completely overlapped with each other, indicating that the extracted TROPOMI time series is not sensitive to SZA thresholds for QC.

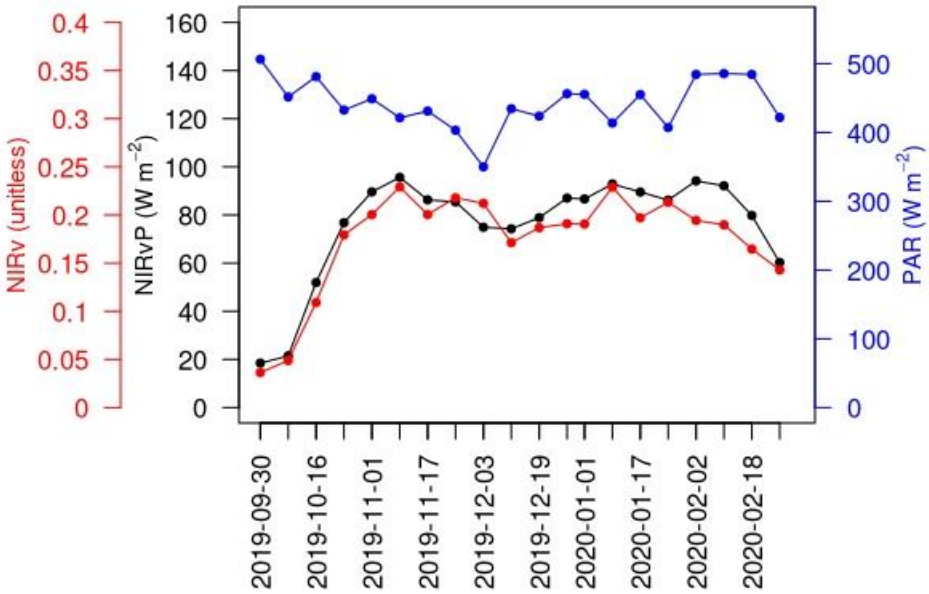

Figure S4: Time series of in situ incoming PAR (blue), NIRv (red), and NIRvP (= NIRv × PAR, black) from October 2019 to February 2020. The data was extracted at 13:30 ± 30 min local solar time and aggregated to 8-day intervals.

Figure S5: PhenoCam images at Kapiti on (a) 5 November 2019, (b) 16 December 2019, and (c) 8 February 2020. Some grasses reached the maturity stage in mid-December due to excessive water availability, while a second peak occurred in February 2020.

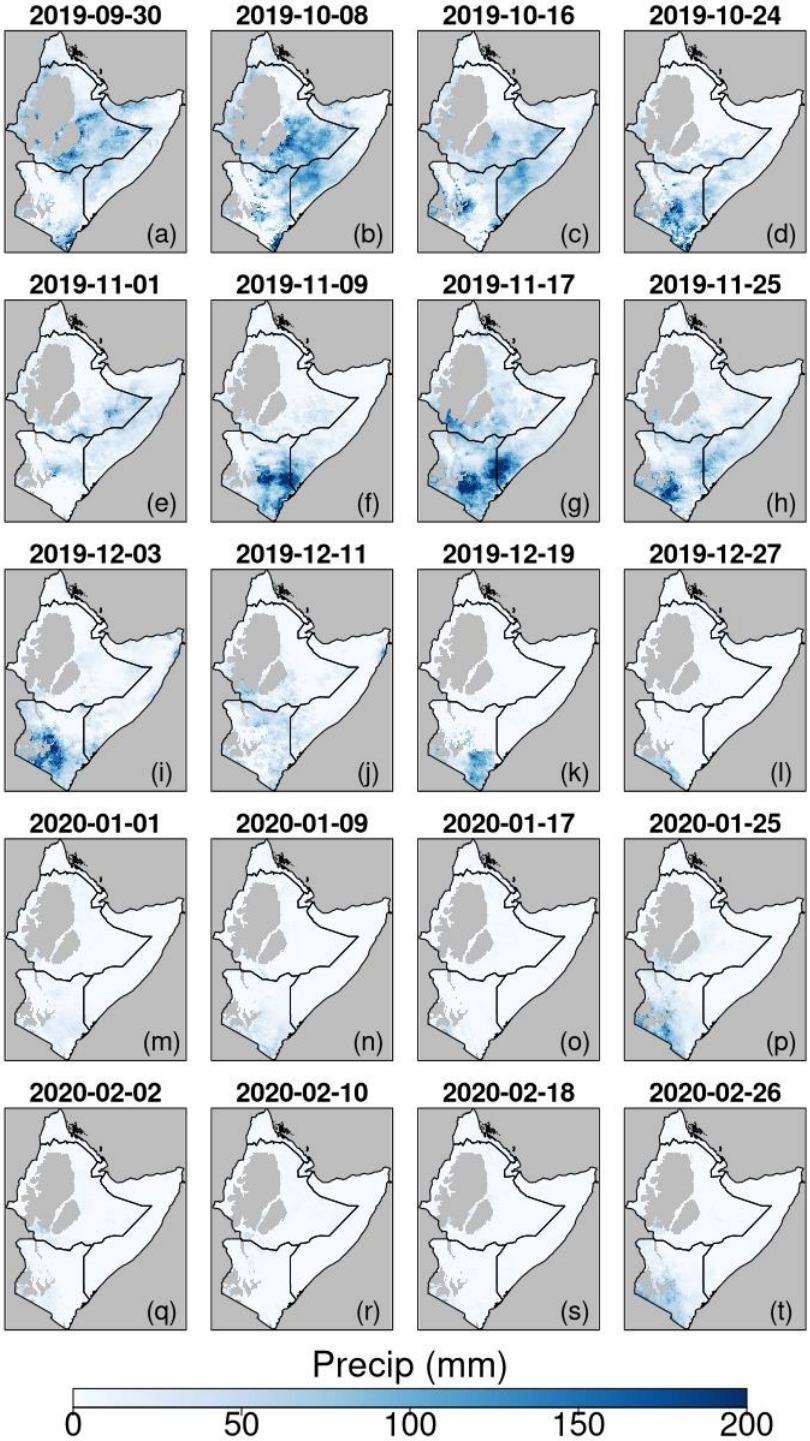

Figure S6: Spatial maps of precipitation in the HoA drylands during October 2019 and February 2020. The date labels represent the starting date of each 8-day period.

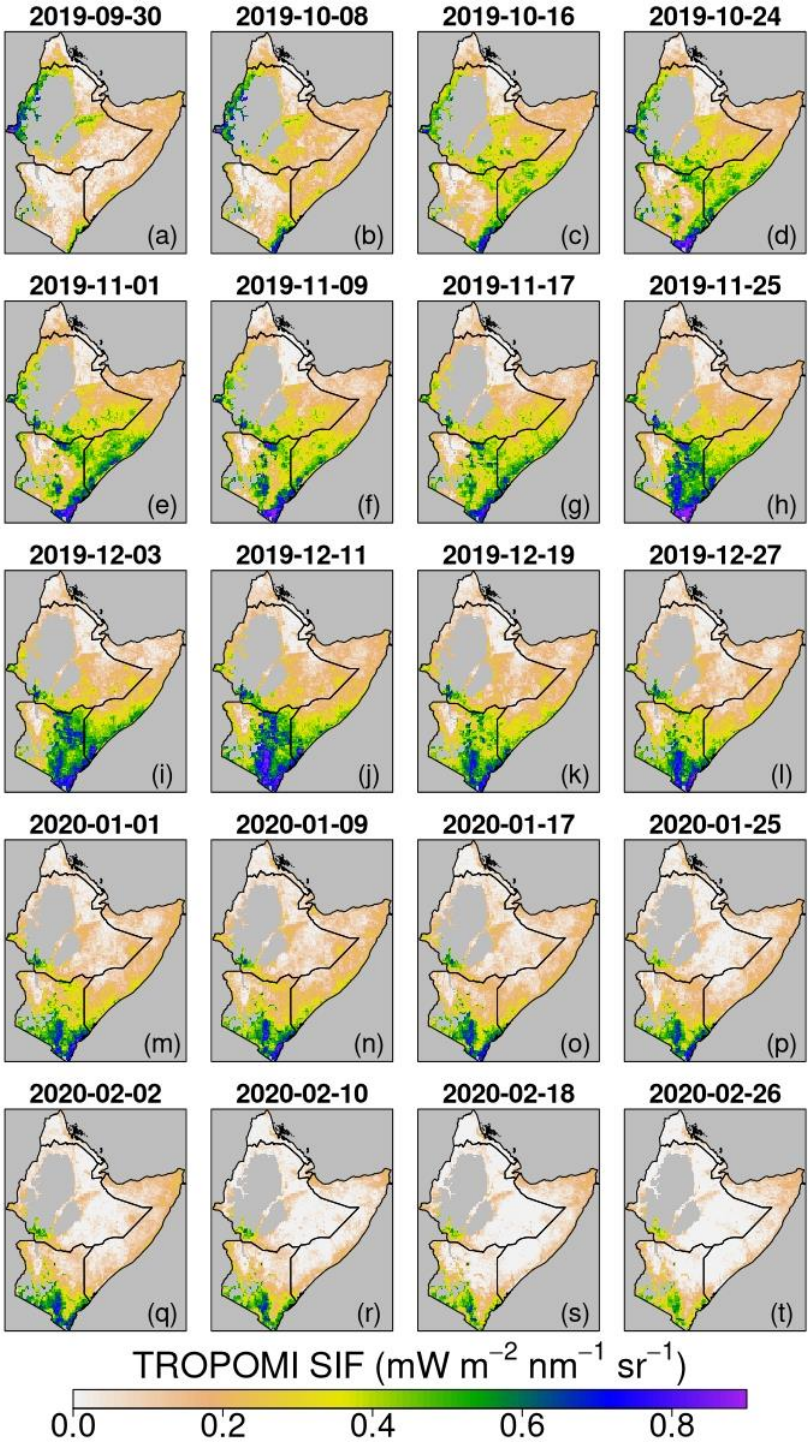

Figure S7. Spatial maps of TROPOMI SIF in the HoA drylands during October 2019 and February 2020. The date labels represent the starting date of each 8-day period.

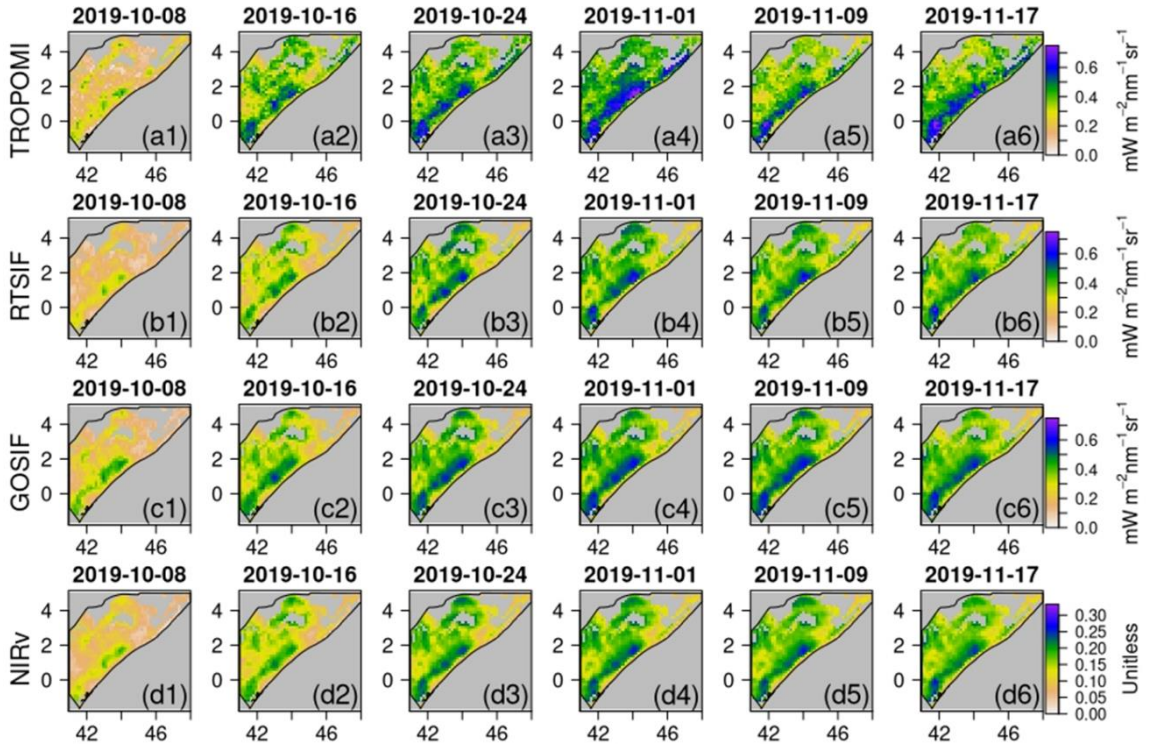

Figure S8. Intra-seasonal variations in (a) TROPOMI SIF, (b) RTSIF, (c) GOSIF, and (d) MODIS NIRv in the grasslands of Region 2 during 8 October and 17 November 2019. The date labels represent the starting date of each 8-day period.

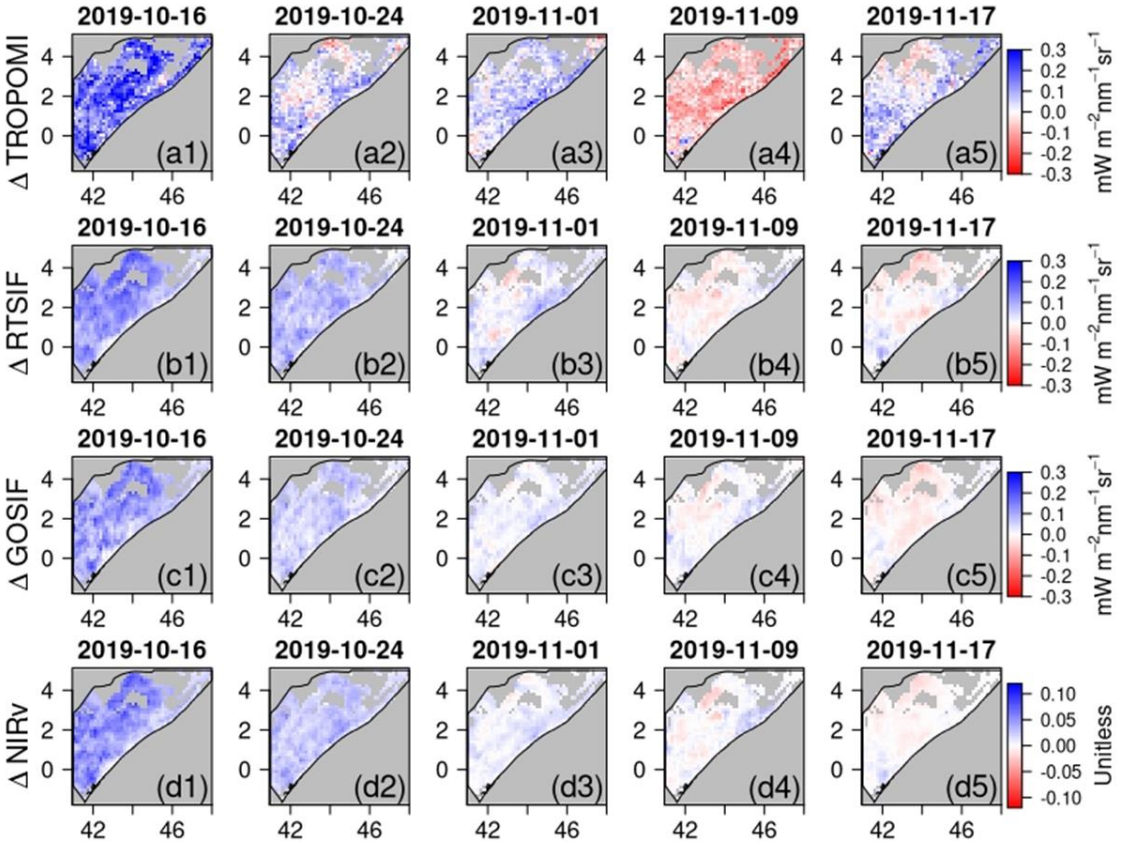

Figure S9: Temporal change rate of (a) TROPOMI SIF, (b) RTSIF, (c) GOSIF, and (d) MODIS NIRv in the grasslands of Region 2 compared to the previous 8-day period during 16 October and 17 November 2019. The date labels represent the starting date of each 8-day period.

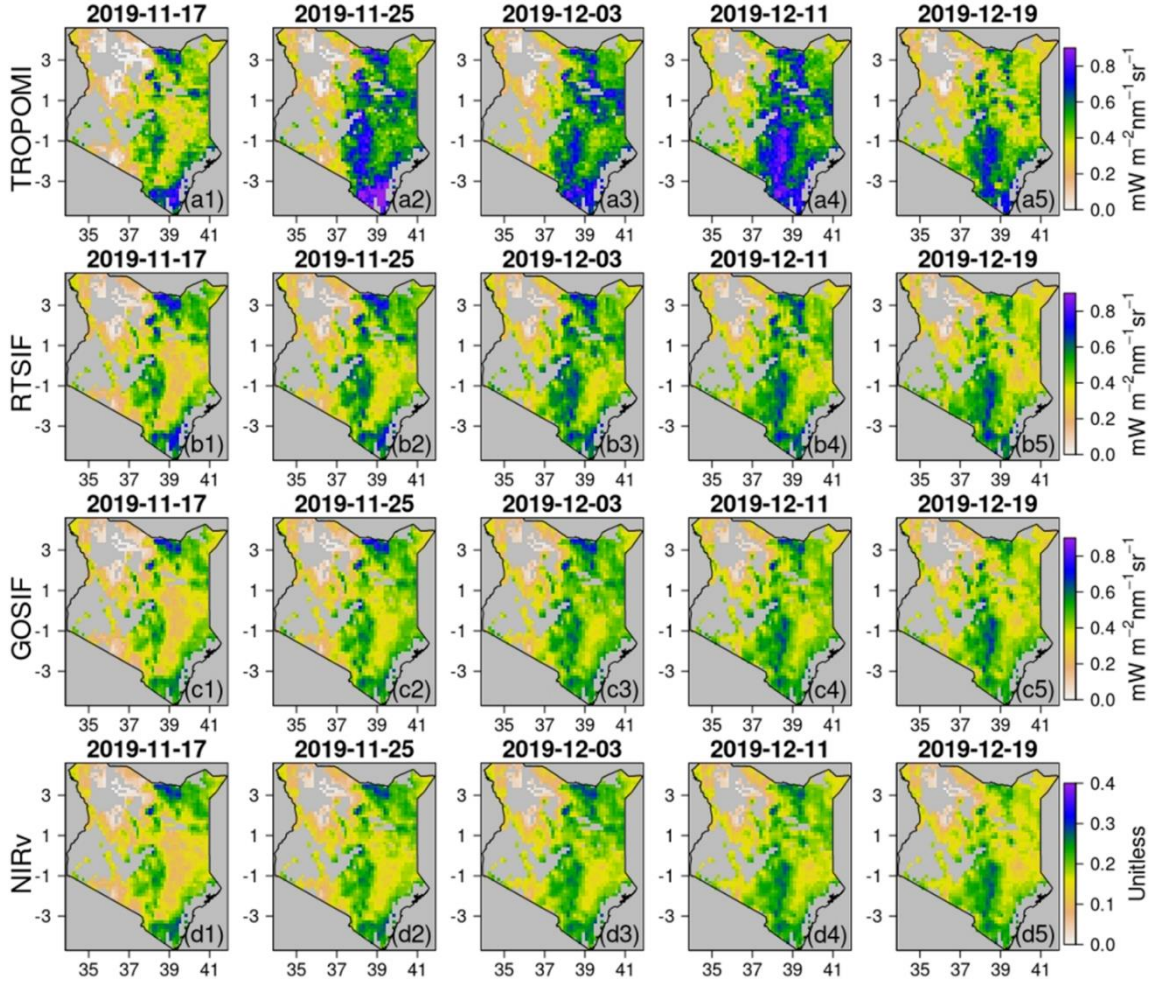

Figure S10: Intra-seasonal variations in (a) TROPOMI SIF, (b) RTSIF, (c) GOSIF, and (d) MODIS NIRv in the grasslands of Region 3 during 17 November and 19 December 2019. The date labels represent the starting date of each 8-day period.

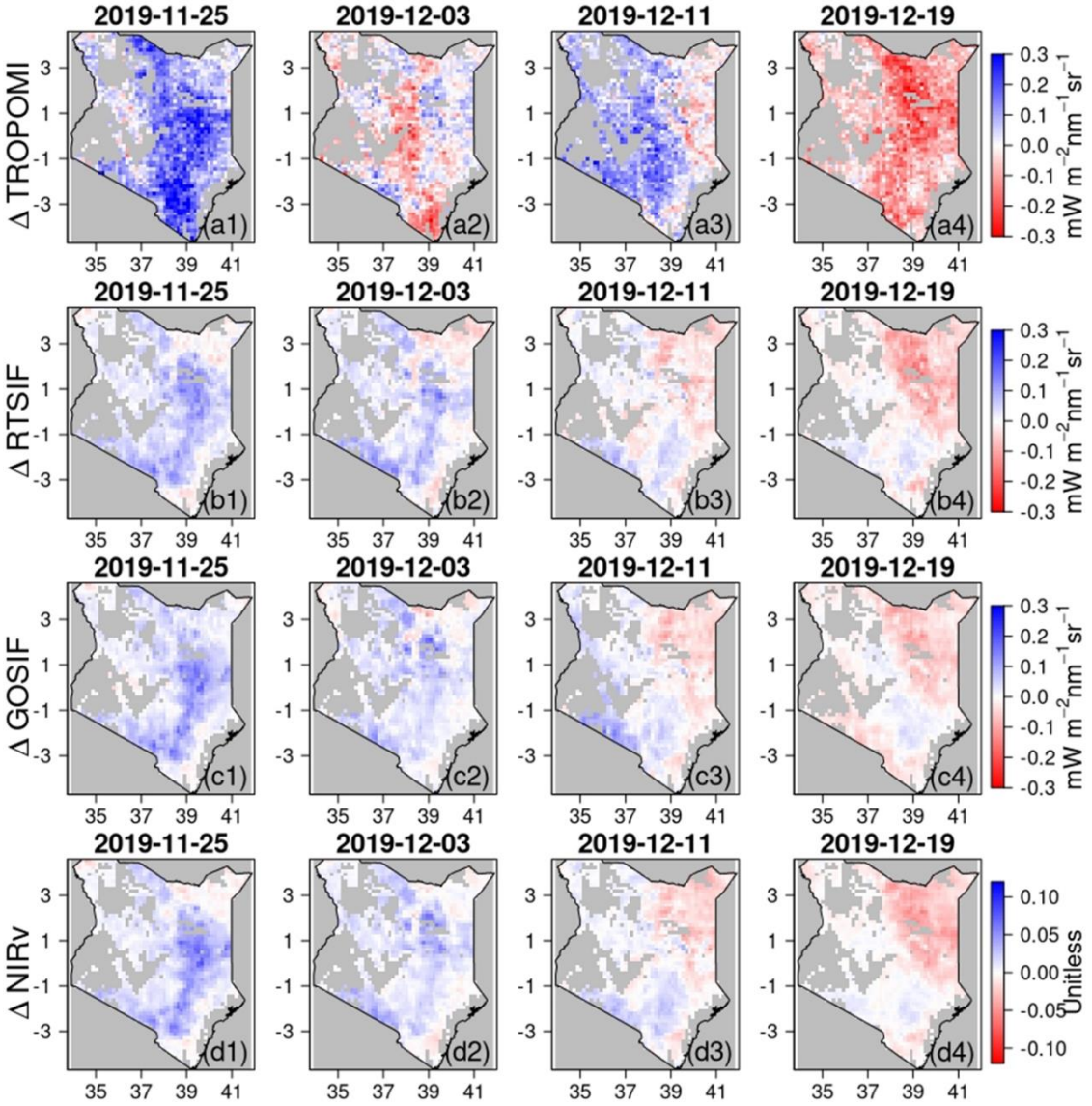

Figure S11: Temporal change rate of (a) TROPOMI SIF, (b) RTSIF, (c) GOSIF, and (d) MODIS NIRv in the grasslands of Region 3 compared to the previous 8-day period during 25 November and 19 December 2019. The date labels represent the starting date of each 8-day period.

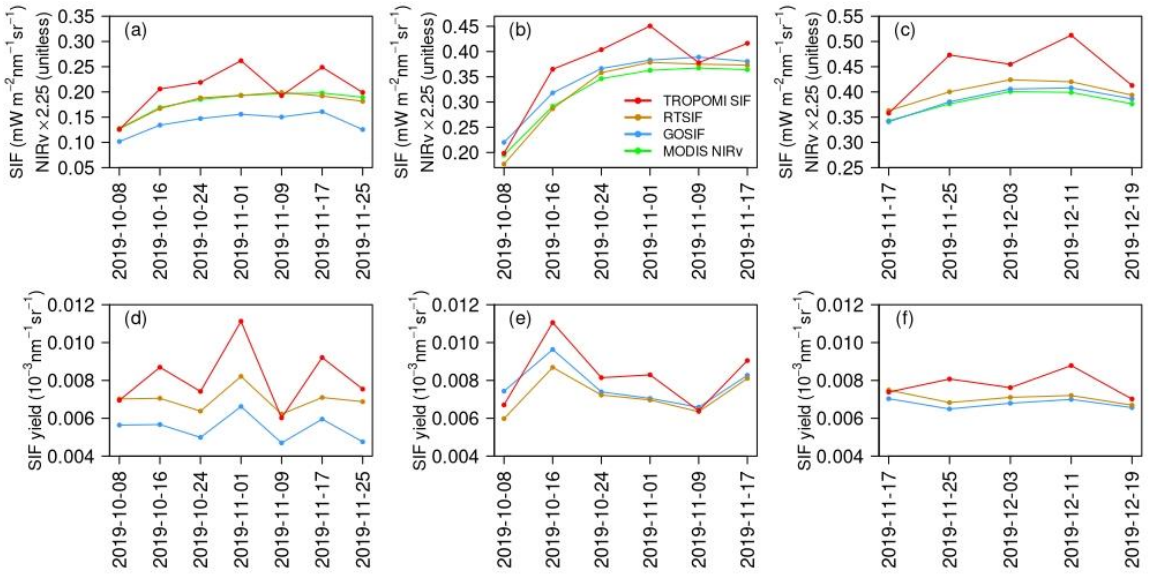

Figure S12: Intra-seasonal variations in (a–c) SIF or NIRv and (d–f) SIF yield for the three sub-domains during the selected time windows (Fig. 4). The x axis labels represent the starting date of each 8-day interval.